the society for solid-state
and electrochemical
science and technology

Journal of The Electrochemical Society

Pt_xCo_y Catalysts Degradation in PEFC Environments: Mechanistic Insights: II. Preparation and Characterization of Particles with Homogeneous Composition

Pascal Fugier, Sylvain Passot, Christelle Anglade, Laure Guétaz, Nicolas Guillet, Eric De Vito,
Sophie Mailley and Alejandro A. Franco

J. Electrochem. Soc. 2010, Volume 157, Issue 6, Pages B943-B951.
doi: 10.1149/1.3385000

Journal of The Electrochemical Society, **157** (6) B943-B951 (2010)
0013-4651/2010/157(6)/B943/9/$28.00 © The Electrochemical Society

Pt_xCo_y Catalysts Degradation in PEFC Environments: Mechanistic Insights

II. Preparation and Characterization of Particles with Homogeneous Composition

Pascal Fugier,[a,z] Sylvain Passot,[a] Christelle Anglade,[a] Laure Guétaz,[b] Nicolas Guillet,[b] Eric De Vito,[b] Sophie Mailley,[c] and Alejandro A. Franco[a,*,z]

[a]Laboratoire des Technologies des Surfaces, Département des Technologies des Nanomatèriaux, [b]Laboratoire des Composants pour Piles à Combustibles et de Modélisation, Département de l'Electricité et de l'Hydrogène pour les Transports, and [c]Laboratoire des Batteries Avancées, Département de l'Electricité et de l'Hydrogène pour les Transports, Commissariat à l'Energie Atomique et aux Energies Alternatives/ Centre de Grenoble LITEN, 38054 Grenoble Cedex 9, France

---

In this paper, we present experimental results on the preparation and the electrochemical characterization of Pt_xCo_y electrocatalytic particles with homogeneous composition, modeled by Franco et al. [*J. Electrochem. Soc.*, **156**, B410 (2009)]. Preparation is made through the direct liquid injection metallorganic chemical vapor deposition technique previously developed at CEA, and electrochemical analysis is carried out by using a rotating disk electrode and membrane-assembled gas diffusion electrode. Degradation structural changes are characterized by using transmission electron microscopy, X-ray diffraction, and X-ray photoelectron spectroscopy. Optimal Co compositions are identified for better oxygen reduction reaction activity and durability, validating the modeling studies.

[DOI: 10.1149/1.3385000]

Manuscript submitted September 4, 2009; revised manuscript received March 15, 2010. Published May 3, 2010.

The specific activity and stability of polymer electrolyte fuel cell (PEFC) electrodes can be improved by alloying Pt with some transition metals (e.g., Co, Ni, and V). These electrodes therefore achieve lower overall Pt loadings compared to pure Pt-based electrodes. In our previous paper,[1] we have proposed a multiscale kinetic model describing the oxygen reduction reaction (ORR) activity and degradation of Pt_xCo_y nanoparticles in PEFC environments. This model provides mechanistic insights on the impact of the nanostructure and operating conditions on the Pt_xCo_y nanoparticles durability. On the basis of ab initio data, we identify favorable pathways of the ORR on Pt_xCo_y nanoparticles and of the competitive Pt–Co dissolution in acidic media. The derived ab initio-based kinetics is coupled to a description of the atomic reorganization at the nanoparticle level as a function of the cumulated Pt and Co mass losses. This nanoscale model is coupled with a transport microscale model of charges and O_2 through a PEFC cathode, and sensitivity simulations to several operation conditions and initial compositions/ morphologies are performed. Two kinds of particles are simulated:

1. Annealed Pt_xCo_y nanoparticles (representative of complete alloys) by using the Monte Carlo method.
2. Homogeneous Pt_xCo_y particles, i.e., with the surface composition equal to the volume composition (representative of bulk-truncated structures or incomplete alloys).

In this paper, we focus on the preparation and the electrochemical characterization of the second kind of Pt_xCo_y particles. The goal here is not to prepare highly active and stable electrocatalytic systems but to prepare model electrodes with structures/morphologies that can be compared with the Pt_xCo_y homogeneous particles that we modeled in Ref. 1.

Preparation methods for pure Pt or Pt-based electrocatalysts are generally aqueous methods using various reducing agents. The conventional method consists in depositing Pt on carbon and then Co on Pt/C.[2-4] For example, Xiong and Manthiram synthesized Pt–M (M = Fe, Co, Ni, and Cu) catalysts by using a commercial Pt catalyst supported on carbon black.[2] Two other synthesis methods are presented in Ref. 5 and 6. Li et al. developed a method for the synthesis of Pt–Co based on the preparation of a Co/C composite support followed by removing the excess Co in a H_2SO_4 solution.[5]

Other methods based on surface technologies have also been studied such as the chemical vapor deposition (CVD) process. Chemical deposition processes used for the formation of thin films or supported nanoparticles are based on chemical reactions between inorganic or organic metal-containing species, leading to the formation of a thin layer on an appropriate substrate. All these processes are one-step processes, in general, simpler and less expensive than physical deposition processes. They are commonly used for the production of various coatings (metals, oxides, and composites), the main advantage being that they allow an easy scaling up to large size systems and a conformal coverage of complex shapes. The chemical reactions used in CVD are numerous and include thermal decomposition (pyrolisis), reduction, hydrolysis, and oxidation, which can be used either singly or in combination. These reactions can be activated by several methods, the most important one being thermal activation and plasma activation. Depending on the applications and specifications, the reactants (precursors) have to be correctly chosen from the following general groups: halides, carbonyls, metallorganics (MOs), and hybrids.

In our group at CEA, a modified CVD method, the metallorganic chemical vapor deposition (MOCVD) process, has been developed to prepare PEFC electrodes directly on a gas diffusion layer (GDL) support.[7-9] MOs are compounds in which the atom of a metallic element is bound to one or more carbon atoms of an organic hydrocarbon group. Most of the elements used in MOCVD are from the IIa, IIb, IIIb, IVb, Vb, and VIb groups.

In an MOCVD process, thin films or nanoparticles are formed on a surface from the thermal decomposition of the gaseous precursor molecules. The total pressure used in the gas phase is generally a low pressure, in the range of a few Torrs.

Precursors for MOCVD should, in general, have an evaporation rate that is high enough, stable, and constant in time. The precursor molecule should be chemically and thermally stable during the transport through the gas phase to the surface. The precursor should be

1. Relatively easy to synthesize.
2. Not be dangerous and should not produce dangerous products.
3. Must be soluble and stable in a suitable solvent without formation of precipitates (in a droplet-derived deposition process).

---

* Electrochemical Society Active Member.

[z] E-mail: pascal.fugier@cea.fr; alejandro.franco@cea.fr

Classical MOCVD processes are based on the evaporation of solid MO precursors and meet the problem of irreproducibility of vapor generation and transport, thus making the growth process and consequently the film properties less reproducible. Due to these reasons, new liquid delivery systems have been introduced a few years ago to overcome the problem of thermal stability of some complexes such as the pulsed liquid injection metallorganic chemical vapor deposition (PLI-MOCVD) process or the direct liquid injection metallorganic chemical vapor deposition (DLI-MOCVD) process.[10-12] The main advantages of these liquid delivery systems are:

1. A single precursor mixture can be used for multi component systems.
2. Very high growth rates can be obtained.
3. Precursors (solid or liquid) can be kept at low temperature and atmospheric pressure.
4. Only small amounts of materials (a few microliters) are volatilized.

The evaporation of precursors with low vapor pressure even under atmospheric pressure is possible. In PLI-MOCVD, the solution is injected directly by a microvalve. The injector injects microdoses (a few microliters) of an organic solution containing a dissolved mixture or a pure MO liquid precursor. After flash evaporation, the resulting vapor mixture is transported by gas toward the heated substrate. The frequency, the opening time, and the solution concentration are the main parameters controlling the growth rate. To date, on the basis of this liquid delivery system, high quality noble metal nanoparticles or oxide films have been obtained in our institute.[13] This method is very versatile and is thus suitable for in situ deposition of thin films or complex systems such as metal/oxide composites, carbon nanotube, nanoparticles, and multilayers.

In this paper, we discuss the structural and electrochemical properties of model Pt_xCo_y PEFC cathodes made using the DLI-MOCVD process depositing on a carbon support Pt and Co at the same time. Results are reported for cathodes operated under different operating conditions and operating times. This compliments our modeling work on Pt_xCo_y-based nanoparticles already published in Ref. 1 and 14.

The paper is organized as follows. First, we present the experimental preparation of the cathodes and characterization setups. Second, we discuss the characterization results regarding the activity and stability properties according to the Pt_xCo_y nanostructure, in connection with our previously published modeling results. Finally, we conclude and indicate further directions in our research.

Experimental

Preparation of the Pt_xCo_y electrocatalysts.— Pt_xCo_y electrocatalysts were prepared using the DLI-MOCVD method developed at CEA. For the deposition of the bimetallic electrocatalysts in the reactor, dimethyl(1,5-cyclooctadiene) platinum(II) [$Pt^{II}(Me_2,cod)$, Strem] and cobalt(III) acetylacetonate [$Co^{III}(acac)_3$, Strem] were used as precursors. All precursors are soluble in toluene (Aldrich) for the used concentrations (<0.03 M). Simultaneous liquid injection was done to obtain bulk-truncated or incomplete Pt_xCo_y alloys. The Pt_xCo_y ratio is controlled by the precursor concentration. The precursor solutions were pushed by nitrogen. The solvent was then evaporated and cracked by thermal effect and oxidative atmosphere (O_2 80%, N_2 20%). Both precursors were also decomposed by the temperature and gas pressure inside the reactor (Fig. 1). Pt_xCo_y electrocatalysts were formed at 350°C on a GDL (ELAT LT1400W, E-Tek BASF) playing the role of microporous carbon catalyst support.[d] No ionomer impregnation was applied after the catalyst elaboration to avoid ionomer poisoning effects on the catalysts' electrochemical behavior during the experimental tests.

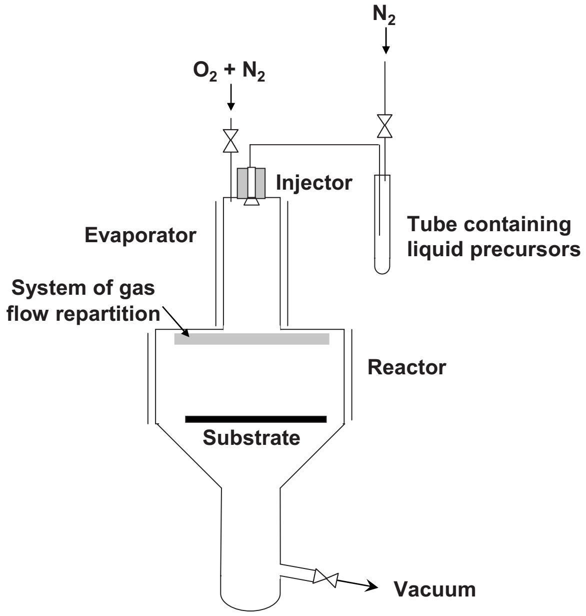

Figure 1. Schematic diagram of the DLI-MOCVD process reactor.

Structural and chemical characterization methods.— The metal loadings in the fresh samples were measured by inductively coupled plasma atomic emission spectroscopy (ICPAES). The morphology and the particle size distribution were observed by electron microscopy [transmission electron microscopy (TEM) and field-emission gun scanning electron microscopy (FEGSEM)]. Observations of the GDL support surface after deposition were performed using a LEO 1530 FEGSEM coupled with an energy-dispersive X-ray spectrometry (EDXS) analysis. TEM images and EDXS analyses were also realized using a JEOL 2000 FX microscope. The particle structures were observed by high resolution transmission electron microscopy (HRTEM) using a JEOL 4000 EX microscope. The X-ray diffraction (XRD) patterns were obtained from a Bruker D5000 diffractometer. The surface of the nanoparticles was characterized by X-ray photoelectron spectroscopy (XPS). The XPS device used in this study consisted of an SSI S-Probe spectrometer equipped with a monochromatized Al Kα source. The pass energy was chosen to be 50 eV while the energy resolution was kept at 850 meV.

Chemical leaching was carried out (24 h, H_2SO_4 0.5 M, 50°C) on the pure Pt catalyst and on the three Pt_xCo_y catalysts to distinguish the dissolution induced by the acidic media from the one induced by the potential cycling. Then, platinum and cobalt were also dosed by ICPAES.

Electrochemical characterization methods.— Our materials were characterized by two electrochemical methods. Rotating disk electrode (RDE) experiments were used first because of their easy implementation and because they allowed us to characterize the catalysts in the most severe conditions of stability. Half-cell experiments were used for fine testing the most interesting materials under conditions closer to the fuel cell environment. Both RDE experiments and half-cell experiments were carried out directly on gas

---

[d] The DLI-MOCVD reactor is a tool dedicated for preparing Pt–Co catalysts. In our catalysts preparation, we have implemented precursors with high purity level (99.9%) and high quality solvents typically used in microelectronics. Based on ICP characterizations, we have not observed any presence of impurities on the fresh catalysts and on the GDL support.

diffusion electrodes (GDEs) (GDE = GDL + catalysts deposit). All the electrochemical experiments were carried out at room temperature in a 0.5 M H_2SO_4 electrolyte.

Ex situ characterizations: RDE performance experiments.— The cell used for the RDE experiments is constituted by a classical three-electrode system with a working electrode consisting of a glassy carbon disk (Sigradur Grade G) supporting our substrate. The counter electrode is a reversible hydrogen electrode (RHE). Before the tests, 1 μL of ethanol was put on the GDE and rinsed with deionized water. The electrochemical three-electrode cell was connected to a digital potentiostat (Autolab PGSTAT30), with an RHE as a reference electrode.

The linear sweep voltamperometry was used to allow the determination of the "electroactive catalyst surface area" (ECSA) (or at least, the H^+ adsorption properties on the catalysts) (under nitrogen bubbling) and to quantify the properties of our catalysts regarding the ORR (under oxygen bubbling). The effective electroactivity of the Pt_xCo_y regarding ORR was determined from voltammetry experiments ($2\ mV\ s^{-1}$) between 1 and 0.4 V_{RHE}. Before each voltammetry, the electrode was kept for 1 min at a potential of 1 V_{RHE} to ensure a reproducible electrocatalytic surface state. During all the experiments, the N_2 or O_2 concentration was kept constant at its saturation value by permanent gas bubbling. The RDE angular rotation rate ω was varied in the 200–900 rpm range. Levich approach is used to calculate the current limited by the convective transport (voltammetry sigmoidal wave height or Levich current)

$$I_L(\omega) = 0.620 \times n \times F \times A_g \times D^{2/3} \times \upsilon^{-1/6} \times C_0 \times \omega^{-1/2} = B \times C_0 \times \omega^{-1/2} \qquad [1]$$

where n is the number of electrons transferred in the ORR, F is the Faraday constant, A_g the is the geometric area of the RDE, D is the O_2 diffusion coefficient, υ is the kinematic viscosity of the electrolyte, C_0 is the O_2 concentration in solution at the bulk level just outside the nanoscopic diffusion layer developed on the catalyst nanoparticle surface (see our atomistic-based nanoscale model in Ref. 1, 14, and 15), and B is the Levich coefficient. The electrode steady-state current $j(E,\omega)$ (A m^{-2} geometric) at a given electrode potential E and angular rotation rate ω is given by the following equation

$$\frac{1}{j(E,\omega)} = \frac{1}{j_k} + \frac{1}{j_L(\omega)} = \frac{1}{j_k} + \frac{1}{nB\omega^{1/2}} \qquad [2]$$

where j_k is the cathodic activation current density at a potential E and $j_L(\omega)$ is the transport-limited current density in the voltammogram (A m^{-2} geometric) derived from Eq. 1.

The RDE voltammogram results presented in this paper display current densities corrected ($j_{corrected}$) by the diffusion in solution using the classical Levich method (for high ORR Butler–Volmer overpotentials, i.e., for $E > 0.8\ V_{RHE}$)

$$j_{corrected} = \frac{j_L(\omega) \times j(E,\omega)}{j_L(\omega) - j(E,\omega)} \qquad [3]$$

Ex situ characterizations: RDE aging test.— Our RDE aging test is analogous to Colón–Mercado and Popov's accelerated durability test[16] where they used a three-electrode system with a Hg/Hg_2SO_4 electrode as the reference electrode. Our aging experiments were carried out at $I = 0$ A (open circuit) for 7 days (160 h) at 60°C in H_2SO_4/0.5 M saturated O_2 electrolyte and using a saturated calomel electrode as a reference electrode connected to an EGG Par 273 digital potentiostat. The same electrochemical characterizations as described above were done before and after aging.

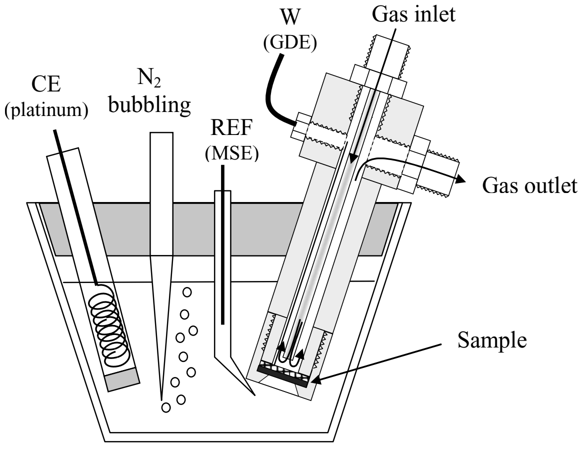

Figure 2. Representation of the three-electrode device for GDE testing (half-cell).

In situ characterizations: half cell performance experiments.— A GDE (14 mm diameter disk) and a Nafion NRE 212 CS membrane (DuPont) were directly bonded together by a hot-pressing process (10 MPa at 150°C for 2 min and 30 s). The obtained membrane electrode assembly (MEA) was inserted in the sample holder with the GDL facing up[17] (Fig. 2). The membrane is then in contact with the liquid electrolyte ($0.50\ cm^2$) while the same surface area of the GDL is fed with the reactive gas. A gold grid provides the electrical contacts and a polytetrafluoroethylene (PTFE) gasket set on the membrane side ensured the tightness of the device.

A three-electrode, two-compartment setup containing 40 mL of H_2SO_4 solution with continuous nitrogen bubbling was used. A platinum mesh was used as a counter electrode, and the reference electrode was in mercury sulfate (mercury sulfate electrode Hg/Hg_2SO_4/0.5 M H_2SO_4 radiometer). Electrochemical experiments were conducted with a digital Bio-logic VMP2 potentiostat. Polarization curves were captured following this test scheme: While the oxygen flow was set at $2\ nL\ h^{-1}$, six voltammetry cycles from 0.05 to 1.15 V_{RHE} at $20\ mV\ s^{-1}$ and one voltammetry cycle at $5\ mV\ s^{-1}$ were performed.

Results and Discussion

Microstructural characterization results on fresh electrodes and aged electrodes.— Atomic Pt/Co volumetric ratios were calculated from ICPAES measurements and compared to EDXS results (Table I). Our DLI-MOCVD process allowed us to obtain very low metal loadings ($<100\ \mu g/cm^2$), making possible materials economies and decreasing cost for possible technology commercialization.

Microstructural characterizations.— Figure 3 shows the FEGSEM images of the four fresh materials prepared by DLI-MOCVD. Atomic ratios were estimated by EDXS. On the pure Pt electrode,

Table I. Compositions of the prepared Pt_xCo_y model electrodes.

	Pt ICPAES loadings ($\mu g/cm^2$)	Co ICPAES loadings ($\mu g/cm^2$)	Pt/Co ratio calculated from ICPAES values	EDXS ($Pt_{L\alpha1}/Co_{K\alpha1}$)
Pt	61	0	100/0	
Pt_3Co	79	9.3	72/28	76/24
PtCo	68	17	55/45	61/39
$PtCo_3$	29	42	17/83	23/77

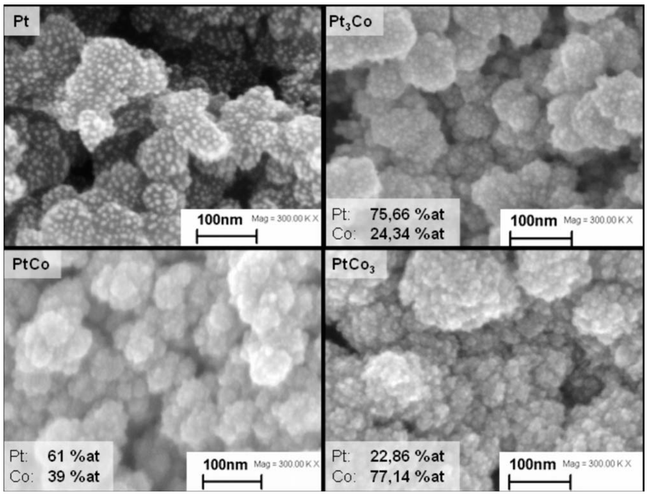

Figure 3. FEGSEM images of the four Pt_xCo_y materials prepared by DLI-MOCVD.

nanoparticles are well-defined and the carbon support is still visible between them. When cobalt is added to platinum, depending on the Pt/Co ratio, the aspect is closer to pure platinum or to pure cobalt, the later growing with a "cauliflower" aspect, probably due to cobalt oxide.

Figure 4 reports the coupled microtome EDXS analysis of the Pt and Co contents inside the GDL. The deposit is present only in the first 5 μm in the GDL thickness with a nonhomogeneous distribution. There is a "crust" at the GDL surface level with a composition close to the expected atomic Pt–Co ratio. However, in depth, the Pt loading appears to be higher.

HRTEM images of Pt_3Co (Fig. 5a) show particle size of around 7–10 nm. The nanoparticles do not have any specific shape. Furthermore, an amorphous oxide layer seems to be present on the nanoparticles (Fig. 5b).

Figure 6 presents the morphology change after the electrochemical aging described in the Electrochemical operation and postaging results section. Before aging, the catalyst particles present a homogeneous distribution. After degradation, the electrode appears to be more porous (higher roughness at the GDL surface), in agreement with our modeling results in Ref. 1 and 14 where the Pt dissolution rate is predicted to be considerably lower than the Co dissolution rate when the two materials coexist at the catalyst (the Pt dissolution rate increases as the Co content at the particle level decreases) and the homogeneous catalyst become more and more like a skeleton-structured particle (the transition element dissolves leaving "holes" in a Pt matrix, like a "French emmental cheese").

XRD structure characterization of the fresh materials.— XRD characterizations provide information about the catalyst crystallographic structure. The diffractograms of all the fresh materials are presented in Fig. 7. The first narrow peak corresponds to the PTFE and the second peak to graphitic carbon, both materials constitutes the GDL. Pure Pt, Pt_3Co, and PtCo diffractograms show the main peaks of the face-centered cubic (fcc) Pt structure. The diffractogram of Pt_3Co also shows a slight shift to higher angles indicating Co insertion inside the Pt crystal lattice. The cobalt atomic fraction alloyed with platinum is calculated from Vegard's law for lattice parameters between a pure fcc platinum and a pure hexagonal close-packed (hcp) cobalt

$$x^{\mathrm{Co}}_{\mathrm{sample}} = \left(\frac{a_{\mathrm{sample}} - a_{\mathrm{Pt,fcc}}}{a_{\mathrm{Co,hcp}}\sqrt{2} - a_{\mathrm{Pt,fcc}}}\right) \qquad [4]$$

Where a_{sample}, $a_{\mathrm{Pt,fcc}}$, and $a_{\mathrm{Co,hcp}}$ are the lattice parameters of the sample (3.893 nm), the pure fcc platinum (3.923 nm), and the pure hcp cobalt (2.506 nm). We find that only about 8% of cobalt is

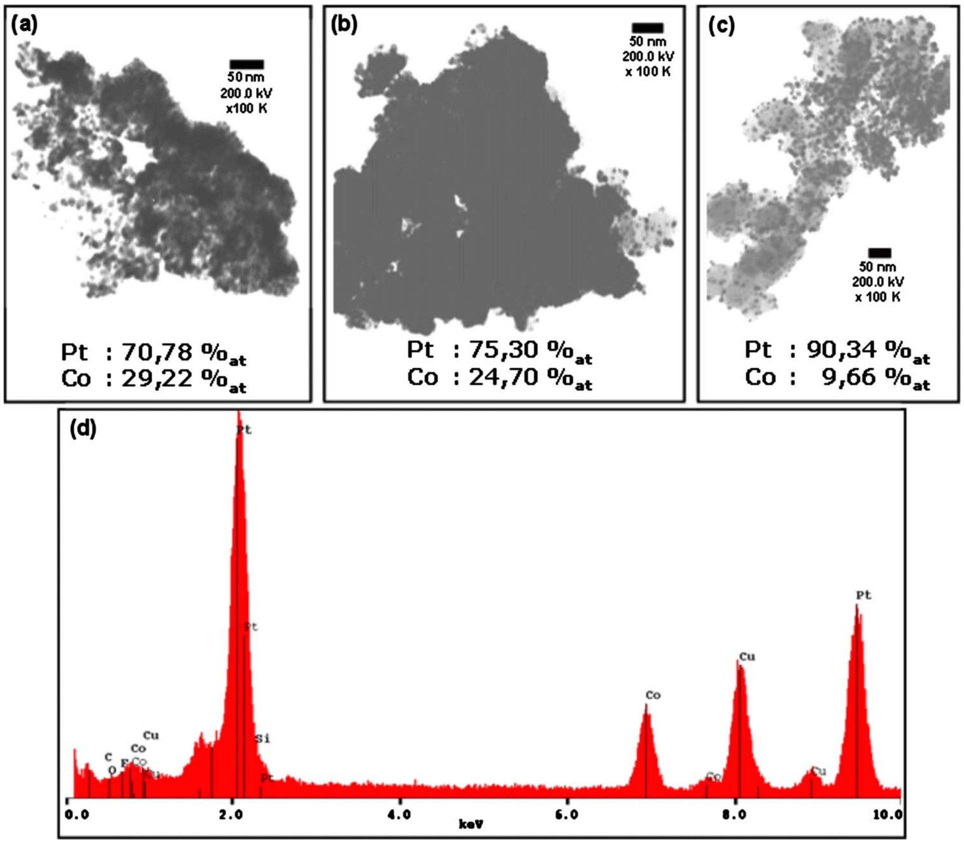

Figure 4. (Color online) [(a), (b), and (c)] EDXS results on fresh Pt_3Co catalysts presented with their associated TEM images. The spectrum (d) corresponds to the image (b). The Cu element appears because of the TEM grid.

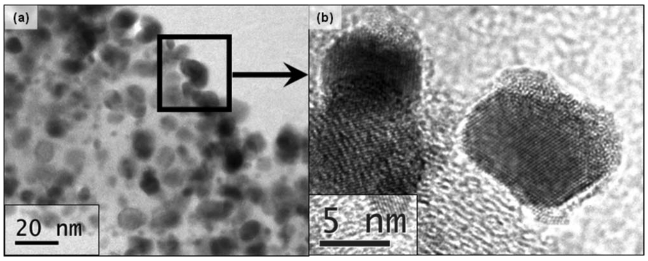

Figure 5. HRTEM images of Pt_3Co nanoparticles elaborated by DLI-MOCVD on a GDL support.

alloyed with platinum in the fresh Pt_3Co sample. The result is analogous for the fresh PtCo sample. The diffractogram of fresh $PtCo_3$ does not show the same main peaks. The peaks of the platinum pattern are lost within the GDL background signals.

These characterization results provide a signature of homogeneous composition (bulk truncated or incomplete alloy) inside these catalysts.[1,14]

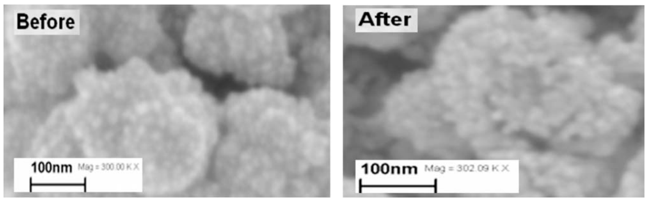

Figure 6. FEGSEM images of the Pt_3Co material elaborated by DLI-MOCVD before and after aging.

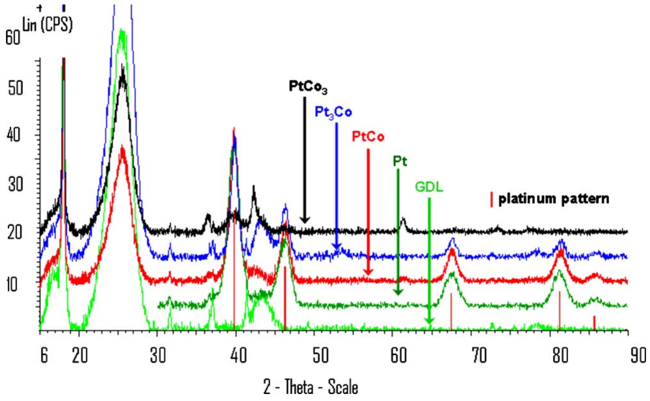

Figure 7. (Color online) XRD spectra of the Pt_xCo_y materials deposited on the GDL by DLI-MOCVD.

XPS surface characterization of the fresh electrodes.— The formation of an oxide layer on the Pt_xCo_y particles should be strongly favored with respect to the conditions of preparation and the oxidation state of the cobalt precursor. This hypothesis is confirmed by the XPS analyses: metallic cobalt (778–778.5 eV)[18-21] is not detected on fresh Pt_xCo_y samples. Instead, a wide peak appears at 781 eV (Fig. 8a), showing the presence of a thick layer of Co oxides (~781 eV).[22,23] However, the abrasion of this oxide layer leads to the apparition of a peak at 778.9 eV (considering the calculated sputtering yields of Pt, Co, and O elements for 500 eV Ar ions,[24] preferential abrasion of oxygen is negligible) (Fig. 8b). This result is coherent with our expectations and our model, which assumes initial oxide coverage in Ref. 1 and 14, as is the case for Pt_3Co in Ref. 25.

XPS surface characterization of the aged electrodes.— XPS analysis on aged electrodes showed unambiguously that the Co disappears from the nanoparticle composition after RDE aging experiments, regardless of their initial composition. Figure 9 compares the survey spectra recorded before and after aging for the $PtCo_3$ sample. After electrochemical aging, no Co peak (around 780 eV) is visible.

As presented in our previous paper,[14] the intensity of the XPS Pt signal after aging depends on the initial composition. For pure Pt, the signal intensity is smaller meaning less metal is visible on the surface after than before. For the three bimetallic catalysts, because of the Co dissolution and of its disappearance from the surface, the Pt signal intensity is greater after than before.

In addition, the XPS analysis after abrasion confirms the hypothesis of a homogeneous profile (bulk-truncated structure or incomplete alloy) in the particles.

Figure 10 shows the O 1s spectra for the three bimetallic materials. Before aging (Fig. 10a-c), two contributions are measured, and after aging, only one is measured (Fig. 10d). Considering Fig. 10, the Co is totally dissolved and no signal is observed. This information confirms that on fresh materials, the Co is oxidized (the peak at 530 eV, which corresponds to oxygen bonded to cobalt disappears when the cobalt peaks disappear).

Electrochemical operation and post-aging results.— *Chemical leaching.*— By dosing the Pt and Co dissolved in the acid solution and by comparing these results with the initial loading values, we are able to determine the quantity of catalyst dissolved from the carbon support. The Pt dissolution is inferior to 1% in the four cases. For the three Pt_xCo_y catalysts, the Co quantity dissolved is close to 50% (Pt_3Co: 58%, PtCo: 54%, and $PtCo_3$: 49%). Our analysis shows that metal dissolution is caused by two different effects: acidic media and potential cycling. Thus, even for an initially well-alloyed material, chemical leaching can possibly take place in the PEFC environment that can lead to an electrode enriched in Pt on the surface before polarization. This phenomenon, occurring without polarization, is not explicitly accounted for in our model in Ref. 1 and 14 (focused on understanding the material degradation under polarization conditions, including open-circuit voltage conditions, i.e., zero total current) but has been recently modeled by ourselves in Ref. 26.

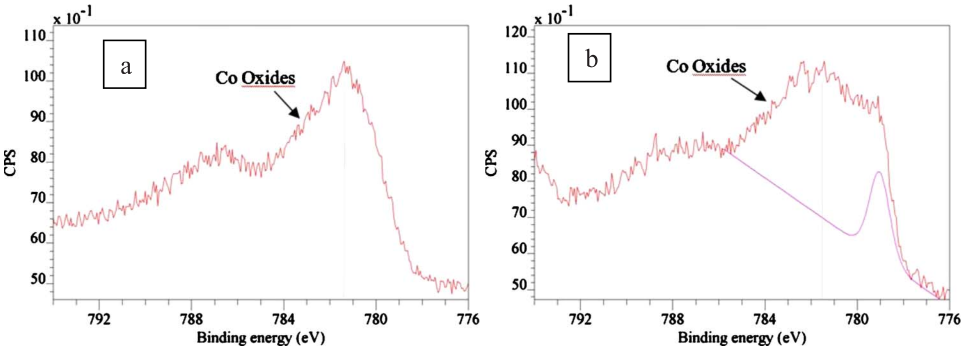

Figure 8. (Color online) XPS spectra of $Co_{2p\ 3/2}$ (a) before and (b) after Ar sputtering ($P_{Ar} = 2.10^{-7}$ mbar, 2kV) the $PtCo_3$ sample surface.

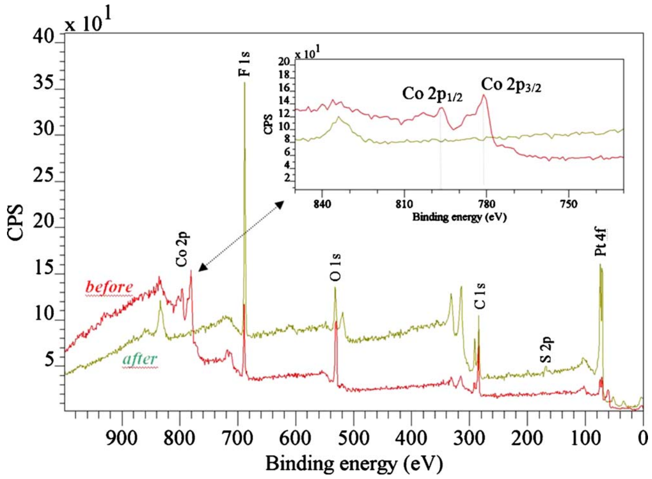

Figure 9. (Color online) XPS survey spectra of the $PtCo_3$ sample, before (green) and after (red) aging.

Ex situ characterizations: RDE performance experiments.— Figure 11 shows cyclic voltamperograms at the beginning of life (BoL) and after the aging of the four tested electrocatalysts. At the BoL, these Pt_xCo_y materials exhibit very different effective ECSA lower to the pure Pt catalyst (Fig. 12a).

The ECSA were calculated by measuring the peak area in the voltammograms and using the following equation

$$\mathrm{ECSA}_{\mathrm{Hupd}} = \frac{Q_H}{q_R} = \frac{A_H/\nu}{q_R} \qquad [5]$$

where A_H is the hydrogen peak desorption area ($\mathrm{C\ V\ s^{-1}}$), ν is the scan rate ($\mathrm{mV\ s^{-1}}$), and q_R is the adsorption charge per cm^2 of platinum on a smooth Pt electrode [assumed to be 210 $\mu C/cm^2$ for a hydrogen monolayer on Pt(111)[27-29]].

We emphasize that this methodology to determine the ECSA based on Eq. 5 only provides a relative comparison of the materials. Rigorously speaking, the "210" value in Eq. 5, derived from an "on-top' adsorption on Pt atoms is unjustified with the Pt_xCo_y catalysts (H^+ can adsorb simultaneously on-top and in bridge between Pt and Co atoms at the Pt_xCo_y catalyst surface and, thus, in a different way compared to pure Pt surfaces). Detailed density functional theory (DFT) studies on adsorption properties of H^+ on Pt_xM_y surfaces are ongoing in our group and are the subject of an ongoing publication.[30]

In the zone of adsorption/desorption, some hydrogen was situated between 0.05 and 0.4 V_{RHE}, three different peaks appeared for all of the considered bimetallic electrodes. These peaks are representative of the adsorption of H^+ on the (110), (111), and (100) crystallographic faces of the platinum and they are very marked (according to Paulus et al.,[31] the insertion of a transition metal leads to poor definition of these peaks). This can indicate that the surface of the particles is Pt-rich.

Figure 12b presents the current densities regarding the ORR as function of the Pt loading for the four tested materials. The current densities provided by the different systems can be ranked as $Pt_3Co > PtCo > Pt > PtCo_3$. We emphasize here that the pure Pt catalyst does not provide the highest current, in contrast to what it could be expected from the ECSA measurement in Fig. 12a. This clearly illustrates that H_{upd} is not an appropriate technique to evaluate the ECSA of the Pt_xCo_y catalysts, as only accounts for H^+ adsorption on Pt sites and as ORR elementary mechanisms on Pt_xCo_y involve both Pt and Co sites.[1,14]

Ex situ characterizations: RDE aging test.— Figure 11 also shows the four cyclic voltamperometries after electrochemical aging of the DLI-MOCVD electrodes at a high fixed potential (low current conditions) in the presence of O_2. The highest current density loss is measured for the pure Pt catalyst (Fig. 13), and Pt_3Co results to be the most stable material, in agreement with our modeling predictions in Ref. 1 and 14. Pt_3Co and PtCo GDE are both still better than pure Pt GDE after aging, in agreement with our model results for short electrode operation time[1] (for longer times, ≈12 days, according to our model, the Pt_3Co and PtCo performances could become lower than pure Pt).

The $PtCo_3$ electrocatalyst has the lowest current density among the four materials, and it shows the higher degradation of the three

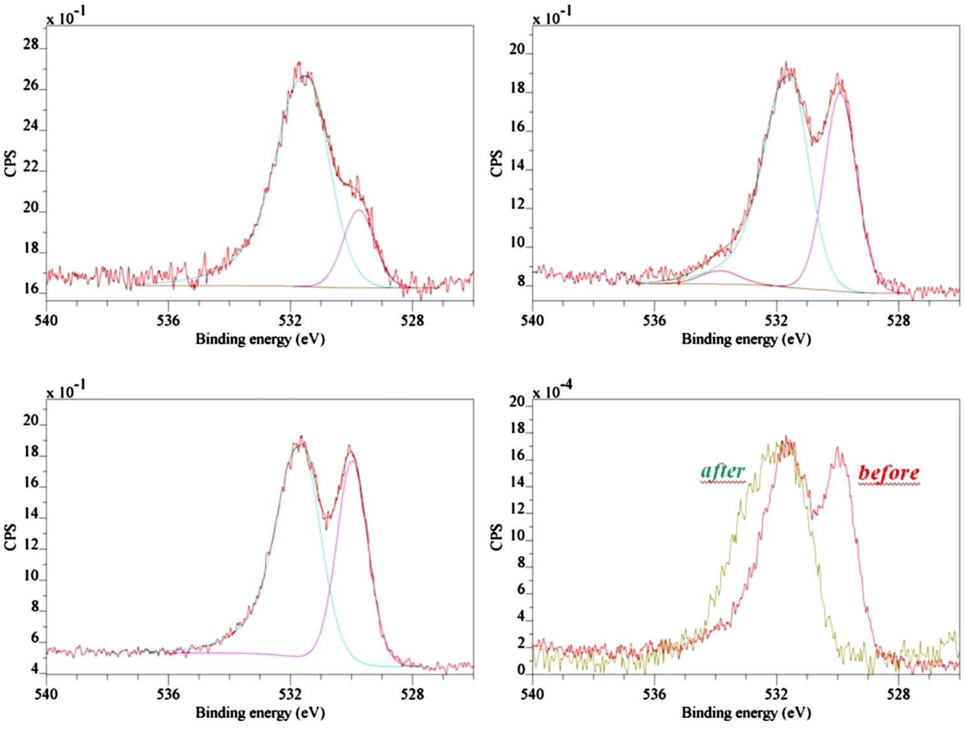

Figure 10. (Color online) [(a), (b), and (c)] XPS oxygen 1s spectra for the three bimetallic electrocatalysts and (d) superposition of the spectra of the PtCo material before and after electrochemical aging.

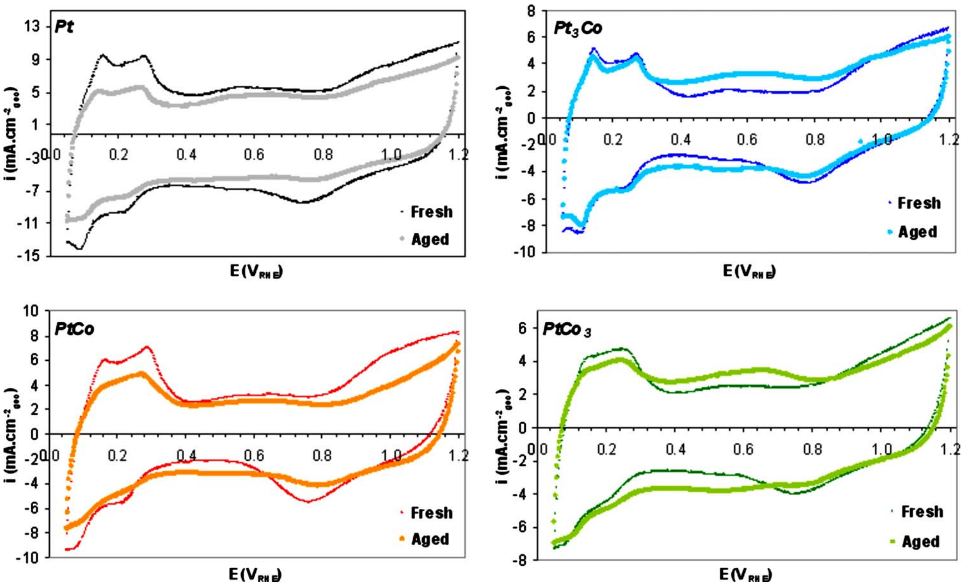

Figure 11. (Color online) Cyclic voltamperograms for the four materials elaborated by DLI-MOCVD, before and after aging at a potential of 0.85 V_{RHE} during 160 h. Nitrogen bubbling, H_2SO_4 0.5 M, 100 mV/s, 900 rpm.

bimetallic materials, in agreement with our modeling predictions in Ref. 1 where we demonstrated, on the basis of ab initio-based elementary kinetics, that the Co dissolution rate is higher (more thermodynamically favorable in acidic media) than the Pt dissolution rate and that the Co dissolution rate is higher for higher Co volume contents. This explains why the stability decreases as the Co volume content increases (i.e., $Pt_3Co > PtCo > PtCo_3$, ranking built here on the basis of the "current loss" signature).

In situ characterizations: half cell performance experiments.— As in RDE experiments, cyclic voltammetry was used here to evaluate the ECSA of the catalysts. In this case, the ECSA are calculated from the hydrogen desorption peak area and from the carbon oxide (CO) stripping peak area. The voltammograms recorded in 0.5 M H_2SO_4 at 298 K and 20 mV s^{-1} scan rate after CO adsorption on pure Pt and illustrate the charges corresponding to desorption of H_{upd} (Q_H) and CO (Q_{CO}). The CO stripping ECSA is calculated from Eq. 5 with $q_R = 420$ $\mu C/cm^2$ representing the charges required to oxidize a monolayer of CO on a Pt electrode.[28,32] As for the H_{upd} methodology, we emphasize that this method only provides a relative comparison of the materials. Detailed DFT studies on the adsorption properties of CO (for the three compositions of PtCo) surfaces are ongoing in our group and are the subject of a future publication.[30,33]

From the calculated values reported in Table II, one can note the quite good agreement of the results obtained by the two methods. It also appears that the values of the roughness factor S_{cat}/S_{geo} (cm^2 Pt/cm^2) are very low compared to typical values reported on MEAs (200–300 cm^2 Pt/cm^2).[34] However, the Pt specific surface area A_{Pt} (m^2/gPt) is of the same order of magnitude such as MEAs, typically 50–80 m^2/gPt.[34]

The relatively high Pt ECSA suggests that the catalyst layer is very thin (in agreement with the microtome analysis discussed in the Microstructural characterization results on fresh electrodes and aged electrodes section) and that a great part of the particles are electrochemically active.

Cyclic voltammetry experiments under O_2 were performed on each sample, prepared and tested in the same conditions to facilitate a direct comparison of the performance of the various catalysts.

Electrochemical impedance spectroscopy (EIS) measurements were also performed on the samples at four current densities: 0.1, 2, 10, and 20 mA cm^{-2}, applying a 0.2 mA cm^{-2} amplitude sinus signal from 10 kHz to 0.2 Hz. Oxygen reduction current curves are presented in Fig. 14. The potentials are corrected for the ohmic loss with the values of the electrolyte resistance, R_Ω (cf. Fig. 16) previously determined by EIS measurements. A semilogarithmic representation (Tafel plot) is given in Fig. 15 showing that the linear evolution of the potential is the same for the three bimetallic catalysts. The slopes are close to 130 mV dec^{-1} whereas it comes near to 120 mV dec^{-1} for pure Pt.[35]

The reduction current of the different catalysts at 0.9 V_{RHE} are given in Table III. Oxygen reduction current corrected with the Pt loading shows similar values for the three PtCo catalysts. These values are closely twice more than for the pure Pt catalyst, showing the improvement on the ORR activity induced by the presence of Co, as already demonstrated with our model.[1,14] Evolutions of the transfer resistance for oxygen reduction vs current density, determined by impedance spectroscopy, are given in Fig. 16.

From these figures, it can be concluded that the best performances are given by the highest Pt-loaded bimetallic samples, in agreement with our modeled polarization curves in Ref. 1 and 14.

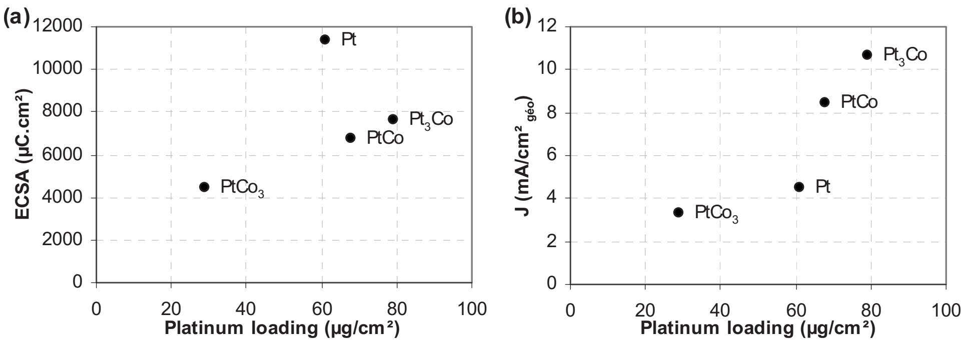

Figure 12. (a) ECSA and (b) current density measured at a potential of 0.85 V_{RHE} plotted as function of Pt loadings for the four prepared materials.

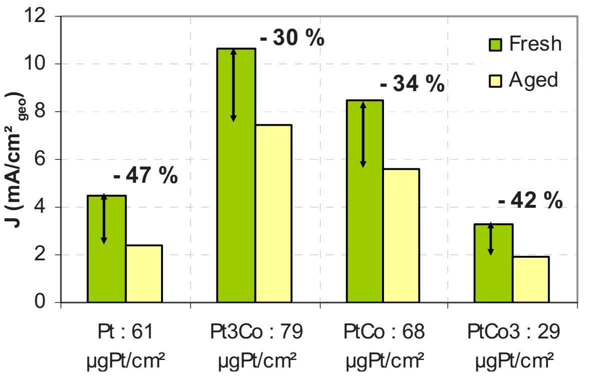

Figure 13. (Color online) Experimental aging results (using Levich equation) for Pt_xCo_y and elaborated by DLI-MOCVD and aged at 0 A during 160 h. The current densities presented here were measured at a potential of 0.85 V_{RHE}.

Table II. ECSA and platinum surface area of the prepared catalysts calculated by hydrogen adsorption (Hupd) and CO stripping voltammograms.

	ECA_{Hupd}		ECA_{CO}	
Catalyst	S_{cat}/S_{geo} (cm^2_{Pt}/cm^2)	A_{Pt} (m^2/g_{Pt})	S_{cat}/S_{geo} (cm^2_{Pt}/cm^2)	A_{Pt} (m^2/g_{Pt})
Pt	20	29	23	34
Pt_3Co	28	40	29	43
PtCo	25	37	27	40
$PtCo_3$	15	22	16	24

Compared to these catalysts, pure Pt shows a 30–40 mV shift toward the anodic potential. Then, the low Pt loaded bimetallic sample curve is still further shifted of approximately 40 mV. The following activity rank can be built, in excellent agreement with our previously published modeling results: PtCo > Pt_3Co > Pt > $PtCo_3$. According to our model, the surface accumulation of HO_2 species is higher for $PtCo_3$ compared to Pt_3Co because of the higher Co surface composition; thus, $PtCo_3$ has a lower overall ORR activity. The number of possible surface transfers of ad-oxygenated species from Pt to Co is maximum at a surface composition of 50–50%, and this explains why homogeneous PtCo offers better ORR activity.[1]

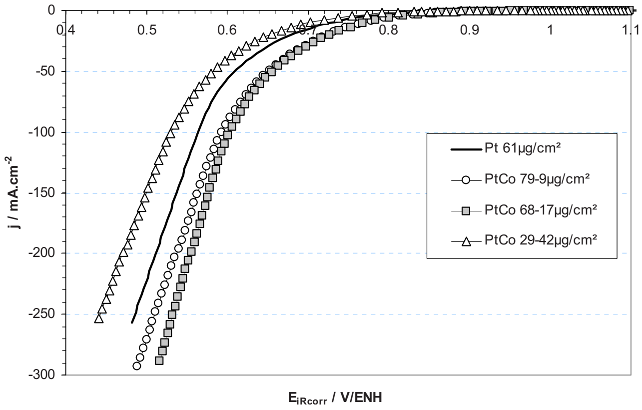

Figure 14. (Color online) i_R-corrected voltammograms (0.5 M H_2SO_4, 25°C, sweep rate of 20 mV s^{-1}). Oxygen reduction current density vs applied potential.

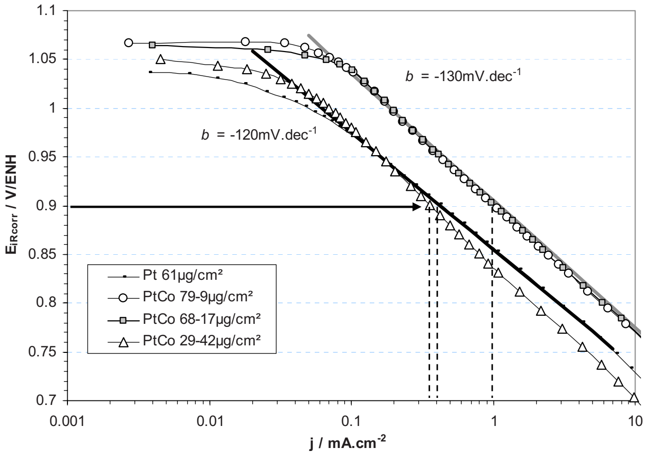

Figure 15. (Color online) Semilogarithmic representation (Tafel plot) of the i_R-corrected oxygen reduction current.

Table III. Reduction current of the different catalysts at 0.9 V_{RHE}.

	Pt	Pt_3Co	PtCo	$PtCo_3$
J_{geo} at 0.9 V($\mu A/cm^2$)	418	1057	1057	360
J_m at 0.9 V(A/g_{Pt})	6.8	13.4	15.5	12.4
J_S at 0.9 V($\mu A/cm^2_{Pt}$)	19	37	41	23

Conclusions

In this paper, we report the experimental results on the preparation and the electrochemical characterization of Pt_xCo_y electrocatalytic particles with homogeneous composition, which we previously modeled in Ref. 1 and 14. We demonstrate that DLI-MOCVD elaborated Pt_xCo_y catalysts supported on a GDL substrate are interesting model systems to understand the electroactivity and stability properties of Pt_xCo_y bulk-truncated or incomplete alloy structures. Electrochemical analysis of the samples has been carried out by using RDE and half-cell experiments. Fresh catalysts and structural changes were characterized by using TEM, XRD, and XPS. An optimal Co composition is identified for better ORR activity and catalyst durability, validating our previously published multiscale model results with kinetic parameters fully obtained by using ab initio DFT data.

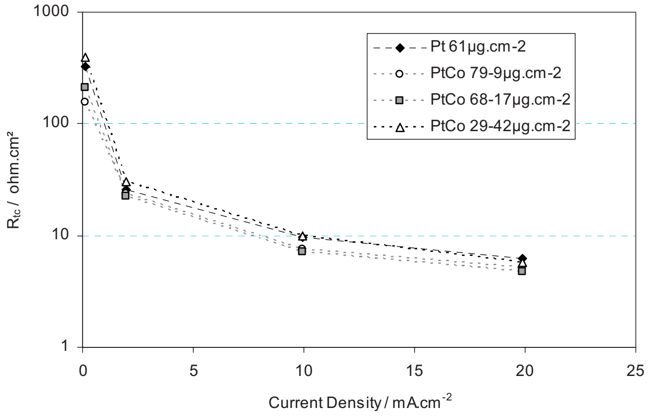

Figure 16. (Color online) Evolution of the transfer resistance for oxygen reduction obtained by impedance spectroscopy vs current density.

These results provide a first indication on the performance and durability of catalysts elaborated by DLI-MOCVD in conditions close to a PEFC cathode. Even if we noted degradation of the Pt_xCo_y under the RDE aging experiments, the Co element apparently slows down the mobility of the Pt on the carbon support, therefore decreasing the electrochemical ripening phenomena.[1] Furthermore, the degree of graphitization of the GDL support possibly plays a role on the activity and stability properties of the prepared catalysts, and this will be the focus of further studies in our group.

Moreover, DLI-MOCVD method can reveal an interesting catalyst preparation technique to achieve ultralow catalyst loadings for PEFC cathodes. To prepare electrochemically stable Pt_xCo_y catalysts, this technique could be combined with thermal annealing ($T > 400°C$) but other carbon supports than GDLs (not thermically stable at $T > 400°C$) should be used. More generally, the preparation of model electrodes and a combined experimental electrochemistry/modeling approach provide interesting insights on the understanding of the Pt_xCo_y electrocatalyst nanostructure impact on their activity and stability properties. Within this context, in an incoming paper[36] we are reporting the preparation of particles with a nanostructure similar to the Monte Carlo-based one modeled in Ref. 1.

Acknowledgments

This work was funded by the ANR PAN-H (French National Research Agency) within the context of the OPTICAT project.

Commissariat à l'Energie Atomique et aux Energies Alternatives assisted in meeting the publication costs of this article.

References

1. A. A. Franco, S. Passot, C. Anglade, E. Billy, L. Guetaz, N. Guillet, E. De Vito, P. Fugier, and S. Mailley, *J. Electrochem. Soc.*, **156**, B410 (2009).
2. L. Xiong and A. Manthiram, *J. Electrochem. Soc.*, **152**, A697 (2005).
3. P. Yu, M. Pemberton, and P. Plasse, *J. Power Sources*, **144**, 11 (2005).
4. S. Koh, C. Yu, P. Ma, I. R. Srivastava, and P. Strasser, *J. Power Sources*, **172**, 50 (2007).
5. X. Li, H. R. Colón-Mercado, G. Wu, J.-W. Lee, and B. N. Popov, *Electrochem. Solid-State Lett.*, **10**, B201 (2007).
6. S. C. Zignani, E. Antolini, and E. R. Gonzalez, *J. Power Sources*, **182**, 83 (2008).
7. S. Thollon, F. Sanchette, S. Valange, E. Guelou, J. Barrault, and H. Guillon, WO Pat. 2002/070130 (2002).
8. S. Mailley, P. Capron, S. Thollon, and T. Krebs, WO Pat. WO 2007/088292 A1 (2007).
9. S. Mailley, F. Sanchette, S. Thollon, and F. Emieux, WO Pat. 2007/088291 (2007).
10. J. P. Sénateur, R. Madar, F. Weiss, O. Thomas, and A. Abrutis, French Pat. 93/08838 (1993) and extended: European Pat. FR94/0000858 (1994).
11. F. Felten, J. P. Senateur, F. Weiss, R. Madar, and A. Abrutis, *J. Phys. IV*, **C5**, 1079 (1995).
12. J. P. Senateur, F. Felten, S. Pignard, F. Weiss, A. Abrutis, V. Bigelyte, A. Teiserskis, Z. Saltyte, and B. Vengalis, *J. Alloys Compd.*, **251**, 288 (1997).
13. S. Thollon, F. Sanchette, and J. Barrault, Abstract 87, The Electrochemical Society Meeting Abstracts, Vol. 501, Quebec City, Canada, May 15–20, 2005.
14. A. A. Franco, S. Passot, C. Anglade, E. Billy, L. Guetaz, N. Guillet, E. De Vito, P. Fugier, and S. Mailley, *ECS Trans.*, **13**(17), 29 (2008).
15. A. A. Franco, P. Schott, C. Jallut, and B. Maschke, *J. Electrochem. Soc.*, **153**, A1053 (2006).
16. H. R. Colón-Mercado and B. N. Popov, *J. Power Sources*, **155**, 253 (2006).
17. N. Guillet, L. Roué, S. Marcotte, D. Villers, J. P. Dodelet, N. Chhim, and S. Tré Vin, *J. Appl. Electrochem.*, **36**, 863 (2006).
18. N. S. McIntyre and M. G. Cook, *Anal. Chem.*, **47**, 2208 (1975).
19. I. Alstrup, I. Chorkendorff, R. Candia, B. S. Clausen, and H. Topsøe, *J. Catal.*, **77**, 397 (1982).
20. S. L. T. Andersson and R. F. Howe, *J. Phys. Chem.*, **93**, 4913 (1989).
21. A. B. Mandale, S. Badrinarayanan, S. K. Date, and A. P. B. Sinha, *J. Electron Spectrosc. Relat. Phenom.*, **33**, 61 (1984).
22. M. Oku and K. Hirokawa, *J. Electron Spectrosc. Relat. Phenom.*, **8**, 475 (1976).
23. B. J. Tan, K. J. Klabunde, and P. M. A. Sherwood, *J. Am. Chem. Soc.*, **113**, 855 (1991).
24. M. P. Seah, *Thin Solid Films*, **81**, 279 (1981).
25. U. Bardi, B. C. Beard, and P. N. Ross, *J. Catal.*, **124**, 22 (1990).
26. A. A. Franco, Abstract 3016, The Electrochemical Society Meeting Abstracts, Vol. 902, Vienna, Austria, Oct 4–9, 2009.
27. J. Wu, X. Z. Yuan, H. Wang, M. Blanco, J. J. Martin, and J. Zhang, *Int. J. Hydrogen Energy*, **33**, 1735 (2008).
28. T. Vidakovic, M. Christov, and K. Sundmacher, *Electrochim. Acta*, **52**, 5606 (2007).
29. A. Lasia, *J. Electroanal. Chem.*, **562**, 23 (2004).
30. R. Ferreira de Morais, D. Loffreda, P. Sautet, and A. A. Franco, *ECS Trans.*, **25**(24), 167 (2010).
31. U. A. Paulus, A. Wokaun, G. G. Scherer, T. J. Schmidt, V. Stamenkovic, N. M. Markovic, and P. N. Ross, *Electrochim. Acta*, **47**, 3787 (2002).
32. H. Gasteiger, N. Markovic, P. Ross, and E. Cairns, *J. Phys. Chem.*, **98**, 617 (1994).
33. S. K. Cheah, P. Gélin, O. Lemaire, and A. A. Franco, *ECS Trans.*, **25**(35), 275 (2010).
34. H. A. Gasteiger, S. S. Kocha, B. Sompalli, and F. T. Wagner, *Appl. Catal., B*, **56**, 9 (2005).
35. http://www.osti.gov/energycitations/servlets/purl/823267-aDW6iD/823267.PDF, last accessed September 3, 2009.
36. E. Quenel, P. Fugier, R. Bouchmila, A. A. Franco, E. Paulliac-Vaujour, L. Guetaz, O. Sicardy, and V. Muffato, In preparation.